In Situ Heat Flow Measurements on the Earth, Moon, and Mars

M. Grott, Institute of Planetary Research, DLR, Berlin, Germany

A. Hagermann, The Open University, Milton Keynes, UK

Introduction

Processes observed on planetary surfaces are controlled by the available energy budget, and the heat present in the planetary interior drives processes such as tectonism, magmatism, and the generation of a magnetic field. In this sense, planets act as heat engines, which convert heat into potential, mechanical, or magnetic field energy. The amount of heat available in the planetary interior is a complex function of the planet's history, and the efficiency with which heat is transported to the surface depends on transport properties in the planetary core, mantle, and lithosphere.

To first order, the initial heat budget available in the planetary interior is determined by the planet's size, as the amount of heat stored during planetary accretion is a strong function of the impact energy deposited by accreting planetesimals. Larger planets are exposed to impactors with higher impact velocities and thus energies, resulting in a larger initial energy budget. Following accretion, gravitational energy is converted to heat during planetary differentiation due to metal-silicate segregation, and larger planets will again release more energy than small ones. Thus, larger planets will in general have higher initial temperatures, and due to their smaller surface to volume ratios, they will also tend to stay hotter during their entire evolution.

Once the initial temperature profile has been established after core formation, the thermal evolution of a planet is governed by the release of radioactive energy in the interior and the transport of heat from the interior to the surface via convection and heat conduction. Ultimately, heat will be radiated to space, in general resulting in net planetary cooling during the later stages of planetary evolution. First order models for the thermal evolution of planets are based on spherically symmetric geometries, and much can already be learned by studying energy conservation and transport in the planetary interior.

Such models parametrize planetary heat loss in terms of the mantle Rayleigh number and while earliest models used scaling laws derived from boundary layer theory (Stevenson et al. 1983; Schubert and Spohn 1990; Spohn 1991), it was later recognized that the temperature dependence of the mantle viscosity can result in the development of a stagnant lid (Solomatov and Moresi 1997; Grasset and Parmentier 1998; Reese et al. 1998). Current parameterizations either treat the stagnant lid separately and consider the mantle to convect like an isoviscous fluid (Grasset and Parmentier 1998), or they parametrize surface heat flow in terms of the whole mantle Rayleigh number including the lid (Solomatov and Moresi 1997; Reese et al. 1998). While the former approach enables the modeling of feedback-mechanisms between lithosphere and mantle dynamics, the latter approach has been extended to treat non-Newtonian rheologies. In addition, latest models also try to parametrize the influence of mantle melting on the efficiency of mantle energy transport (Korenaga 2009; Fraeman and Korenaga 2010).

Figure 1: The InSight lander during assembly, test, and launch operations (ATLO) at the facilities of Lockheed Martin Space Systems. HP³ is mounted on the lander deck towards the backside of the lander behind the seismometer's wind and thermal shield.

Image: NASA/JPL/Lockheed Martin

To calculate the thermal evolution of a planet, energy conservation for the mantle and core are considered, and thermal evolution is then driven by the heat fluxes out of the core and out of the mantle. These can be parameterized using scaling laws. In the case of Mars, scaling laws appropriate for stagnant lid convection need to be employed (e.g., Grasset and Parmentier, 1998), and the growth of the stagnant lid is determined by the energy balance at the lithospheric base (Schubert et al., 1979; Spohn and Schubert, 1982; Spohn and Schubert, 1990; Spohn, 1991). Further, it has been noted early on that the single most important parameter in these calculations is the mantle viscosity (Schubert et al. 1979) and other uncertainties are related to the poorly constrained initial temperature profile.

Figure 2: map of the Urey ratio (solid lines) and surface heat flux in mW/m^2 (dashed lines) as a function of Th and K content obtained from 1-D parametrized models (white circles correspond to the HPE concentrations of the four models in Table 1).

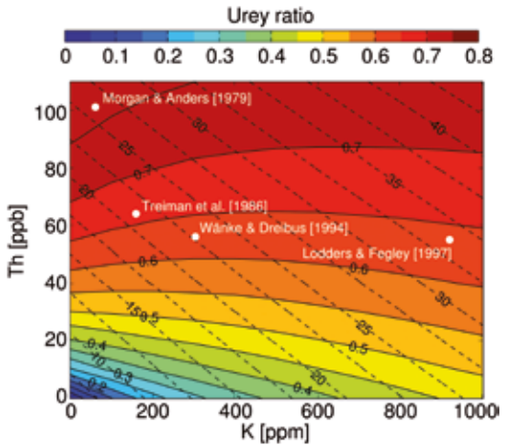

Image: DLR

A useful parameter to describe the effective heat loss of a planet is the so called Urey ratio *Ur*, which quantifies the amount of heat released in the planetary interior in terms of the average surface heat flow. For *Ur*<1, the planet will lose more heat than is released in the interior, and it will cool with time. This is the case for present-day Earth, and is also expected to hold for bodies like Mars and the Moon.

Uncertainties in initial conditions and the unknown mantle viscosity in general require a large parameter space to be studied when investigating a planet's thermal history, but a feedback mechanism between temperature and mantle viscosity reduces the range of admissible present-day thermal scenarios. While high interior temperatures result in low mantle viscosities and fast cooling, low temperatures result in high viscosities and heat accumulation. Consequently, mantle temperatures will tend to similar present day values and heat transport today will be equally efficient almost irrespective of the initial temperature profile provided mantle viscosity is not too large. This so-called thermostat effect enables a direct inversion of the Urey ratio for the heat production rate if the average surface heat flux is known (Plesa et al., 2015).

Table 1: Abundance of heat-producing elements for various compositional models and corresponding heat production rates at the beginning (H0) and end of the evolution after 4.5 Ga (H4.5) (Table 1 of Plesa et al., 2015).

Model	U (ppb)	Th (ppb)	K (ppm)	H_0 (pW/kg)	$H_{4.5}$ (pW/kg)
Treiman et al. (1986)	16	64	160	17	3.7
Morgan and Anders (1979)	28	101	62	21	5.8
Wänke and Dreibus (1994)	16	56	305	23	4.1
Lodders and Fegley (1997)	16	55	920	49	6.1

As an example, results of thermal evolution calculations for Mars using a one-dimensional parameterized evolution model are shown in Figure 2, where a constant *Th/U* ratio of 3.5 has been assumed. The color coded present day Urey ratio is shown as a function of thorium and potassium content and the resulting average present day surface heat flow is shown as dashed lines. Standard cosmo-chemical compositional models for Mars (Morgan and Anders, 1979, Treiman et al., 1986, Wänke and Dreibus, 1994, Lodders and Fegley, 1997) are given as a reference (also summarized in Table 1).

As the simulations show, the present-day Urey ratio of Mars is primarily a function of the mantle thorium content, while it is almost constant as a function of potassium content. This is due to the relatively short half-life of *K* (1.25 Ga), and although Urey ratios can strongly differ during the early stages of the evolution for varying *K* content, they rapidly converge to similar values during the late stage evolution. On the other hand, due to its long half-life, *Th* has a large influence on present day mantle temperatures, and high *Th* contents results in slow mantle cooling and thus large *Ur*. However, if the Urey ratio is assumed to be constant and close to *Ur* = 0.594 ± 0.024 as indicated by thermal evolution models (Plesa et al., 2015), knowledge of the average surface heat flow would allow us to discriminate between cosmo-chemical models. While such measurements are currently missing, the upcoming InSight Mars mission will provide the first baseline measurement at the landing location in Elysium Planitia in 2018.

Terrestrial Heat Flow Measurements

Heat flow directly relates to the rate of cooling a planet is undergoing, and heat flow measurements have been of prime interest for the geophysical exploration of the Earth. Furthermore, heat flow data is instrumental for understanding the working of the planetary heat engine and measurements have been routinely performed on the continents as well as on the ocean floor. The surface planetary heat flow *F* is given by Fourier's law of heat conduction (e.g., Beardsmore and Cull, 2001) and *F* is defined as

$$F = k\frac{\mathrm{d}T}{\mathrm{d}z}$$

where *T* is subsurface temperature, *z* is depth, and *k* is thermal conductivity of the surrounding rock. Therefore, in order to determine *F*, independent measurements of the subsurface temperature gradient as well as the rock thermal conductivity are required (Bullard, 1939, Bullard, 1954, also see Hagermann, 2005, for a review).

In order to properly determine the subsurface thermal gradient, measurements need to be conducted away from surface perturbations. On Earth, these are primarily caused by the diurnal and annual temperature fluctuations, but secular changes in temperature (such as recurring ice ages) can also leave a measurable footprint in the subsurface temperature profile. For periodic temperature forcing, the depth to which these temperature excursions have an effect can be estimated by the thermal skin depth (e.g., Beardsmore and Cull, 2001), which is defined as

$$\mathrm{d}\epsilon = \sqrt{\kappa P/\pi}$$

where κ is thermal diffusivity and *P* is the period of the forcing. Given typical thermal diffusivities of crustal rocks of the order of 10^{-6} m^2/s, annual temperature signals have skin depths of 3-4 m, implying that measurable effects extend to depths of many tens of meters (e.g., Pollack, 1993). Therefore, continental heat flow measurements usually need to be conducted in

Image:

Figure 3: Bullard's penetrator. The eye used for extracting the probe is visible on top of the cylinder housing the temperature recording equipment. Bullard (1954).

boreholes of considerable depths. However, the situation is different when heat flow is measured on the ocean floor, where water temperature is close to constant irrespective of season. In this case, shallow measurements at only a few meters depth are sufficient to reliably determine the thermal gradient, an approach that was pioneered by Bullard (1954).

The classical design of a heat flow probe for marine measurements is shown in Figure 3, and the probe consists of an approximately 5 m long penetrator rod equipped with temperature sensors as well as temperature recording equipment accommodated in a cylindrical housing at the probe's head section (bottom of the image). As probes are deployed from ships and emplace themselves by means of their weight, measurements can only be taken in unconsolidated sediments, which allow the probe to penetrate over the full range of its length.

In addition to the thermal gradient, the thermal conductivity of the surrounding rock needs to be known in order to determine the surface heat flux. For continental heat flow measurements this is usually determined from drill core samples as measured in the lab, thus eliminating the need for high precision thermal property measurements in situ. However, this approach does not usually work for oceanic heat flow measurements as due to the design of the Bullard probe, sediment samples are not automatically available unless a dedicated effort is made to obtain them. Therefore, earliest marine heat flow measurements were usually interpreted by assuming typical sedimentary thermal conductivity values, but the cooldown curve of the penetrator after insertion was also sometimes used to infer the sediment thermal properties. Active heating methods to determine thermal conductivity in situ were only later introduced by Christoffel and Calhaem (1969) and Lister (1970).

An overview of the terrestrial surface heat flow as determined from more than 38.000 individual measurements on the continents and oceans has been compiled by Davies (2013), and a representation of the data is shown as a spherical harmonics model in Figure 4. The average surface heat flow is found to be 91.6 mW m^{-2}, where continents contribute 70.9 mW m^{-2} while oceans show a higher heat flow of 105.4 mW m^{-2} on average. Heat flow is generally lowest in regions of old continental lithosphere like the Scandinavian shield and highest at mid-ocean ridges. The map of surface heat flow therefore strongly reflects the mode of heat transport inside the Earth, with plate tectonics being the dominant process.

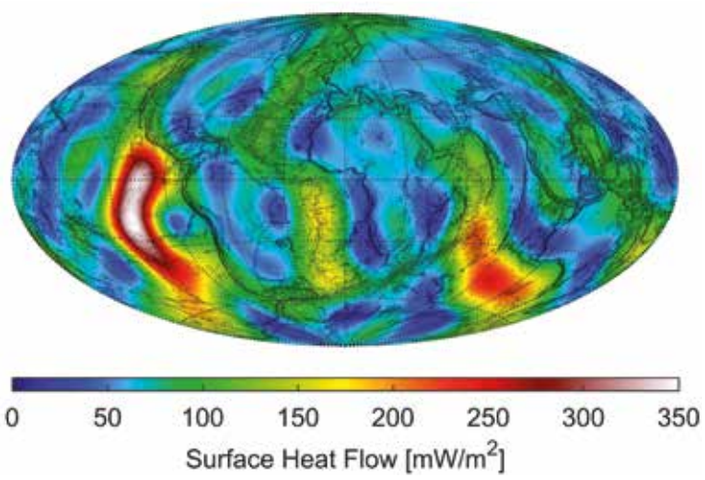

Image: DLR

Figure 4: A spherical harmonics model of the Earth's surface heat flow based on 38,374 measurements, plotted on a shaded relief topographic map.

Lunar Heat Flow Measurements

Apart from the Earth, in situ heat flow measurements have only been performed on the Moon (Langseth et al., 1976), where successful measurements were taken at the Hadley Rille and Taurus-Littrow sites during the Apollo 15 and 17 missions (Langseth et al., 1972a, 1972b, 1973, 1976). While surface temperatures on the Moon vary by up to 300 K over the course of a lunation, drilling to tens of meters into the lunar regolith is not necessary, as the very low thermal conductivity of the lunar regolith efficiently damps the surface temperature signal. Typical thermal diffusivities of lunar regolith are of the order of 10^{-8} m^2/s and thus two orders of magnitude smaller than diffusivities of terrestrial rocks, resulting in thermal skin depths of only around 9 cm. This implies that temperatures are constant and close to their equilibrium value at depths of 1 m and below.

The Apollo heat flow probes were emplaced by astronauts who first drilled holes into the lunar regolith. These were then fitted with a fiberglass bore stem and probes were inserted into the casing. Probes consisted of two identical sections of 50 cm length, each housing two differential thermometers for gradient measurements. Conductivity measurements were made using heaters that surrounded the outer gradient bridge sensors. For redundancy, each experiment consisted of two probes placed a few meters apart. The left panel of Figure 5 shows David Scott emplacing the bore-stem and probe during the Apollo 15 mission, and the final installation of the Apollo 17 probes is shown in the right panel of the same figure.

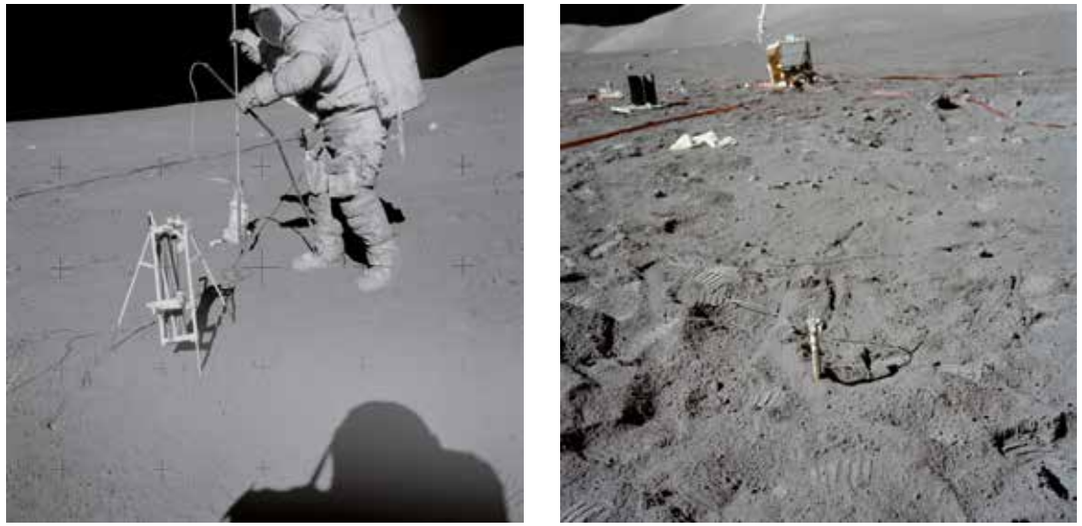

Images: NASA/JSC

Figure 5: Left: David Scott during deployment of the Apollo 15 heat-flow probes. The two-segment probe is in the astronaut's left hand, while the fiberglass bore stem is in his right hand. Bore stem and probe were emplaced in predrilled holes excavated with a hand-held rotary percussion drill system. Apollo photograph AS15-92-12407. Right: One of the Apollo 17 heat flow probes after deployment by Commander Eugene Cernan. The site has been considerably disturbed during instrument deployment. Apollo photograph AS17-134-20496.

The intent for the lunar heat flow measurements was to emplace the probes to a depth of 3 m, but this depth could not be achieved during the Apollo 15 mission due to difficulties while inserting the bore stems into the pre-drilled holes. Rather, bore stems could only be inserted to depths of 1.4 m and 1.0 m on Apollo 15 (Langseth et al., 1972), but these depths were already sufficient to return valuable data. After a mechanical redesign of the bore stem, probes could then be inserted to the designated depth during the Apollo 16 and 17 missions (Heiken et al., 1991).

In total, four attempts have been made to measure lunar heat flow, and the Apollo 13, 15, 16, and 17 missions were equipped with heat flow experiments. The geographical distribution of landing sites is shown in Figure 6, where the surface thorium abundance as measured by the Lunar Prospector Gamma Ray Spectrometer is shown in color code for reference. While the lunar landing of Apollo 13 had to be abandoned due to the explosion of one of its oxygen tanks

en-route, Apollo 14 retargeted the Apollo 13 landing site. However, that mission was not equipped with a heat flow experiment. Further, after redesigning the bore stem in light of the problems faced during the installation of the Apollo 15 experiment, drilling was hugely successful during Apollo 16. However, the heat flow experiment was terminated prematurely when astronaut John Young tripped over the cable connecting the probe to the central electronics and pulled the cable loose from the connector at 121 h and 21 min into the mission (https://www.hq.nasa.gov/alsj/a16/a16.heatflow.html).

Image: DLR

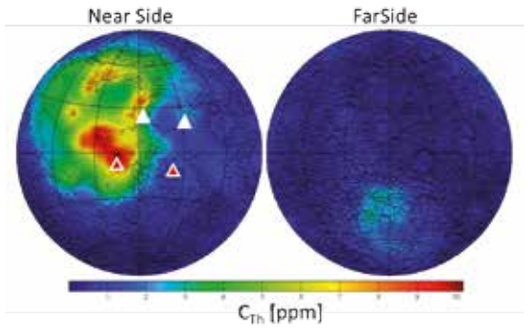

Figure 6: Color coded map of near-surface thorium abundance as measured by the Lunar Prospector Spacecraft. On the lunar nearside, a strong enrichment of Th is visible in a region termed the Procellarum KREEP terraine (PKT). Thorium is also enriched in the Southpole-Aitken basin (SPA) on the lunar farside. Apollo 15 and 17 landing sites are indicated by white triangles, while the Apollo 14 and 16 sites are indicated with red triangles. Apollo 14 retargeted the Apollo 13 site, located in the center of the thorium anomaly.

Therefore, only the measurements at the Hadley Rille and Taurus-Littrow sites were successful, and heat flow values of 21 and 16 mW m^{-2} have been obtained (Langseth et al., 1972a, 1972b, 1973, 1976). Uncertainties for these values are given at ±15%, which mainly stem from the uncertainty connected to the regolith's thermal conductivity. Correcting for local heat flow focusing effects, Rasmussen and Warren (1985) and Warren and Rasmussen (1987) have calculated the globally averaged lunar heat flow, which was found to be 12 mW m^{-2}. From this value, the bulk uranium content of the Moon has been estimated at about 20–21 ppb (Warren and Rasmussen, 1987).

Spherically symmetric (Wieczorek and Phillips, 2000) as well as 3-D thermal evolution models (Laneuville et al., 2013) can reproduce the observed heat flow values by assuming that the observed surface distribution of heat producing elements is representative of the lunar interior, and that the near-surface thorium anomaly termed the Procellarum KREEP Terrane (PKT) is confined to the base of the crust. However, since measurements of lunar heat flow are available only for the transition region between the PKT and the lunar highland terrane, these conclusions remain provisional. Additional information from the center of the PKT (Apollo 13, 14) or the lunar highlands (Apollo 16) would have greatly increased confidence in the obtained results, but as it stands tests of these models will need to await future geophysical exploration missions.

It is worth noting that temperatures recorded at the Apollo sites show some long-term drift, which was originally thought to stem from astronaut-induced perturbances (Langseth et al., 1976, also compare Figure 5), but were later found to persist over the entire duration of the mission and did not develop into a new equilibrium thermal state as expected (Wieczorek and Huang, 2006; Saito et al., 2007). So far, no conclusion concerning the cause of the perturbation has been reached, and different causes for the temperature increase including the 18.6 year precession cycle as well as topographic effects have been considered (Wieczorek and Huang, 2006; Saito et al., 2008). Again, addressing this problem will likely require new measurements to be made in situ.

Measuring the Martian Planetary Heat Flow

Up to now, no direct measurements of the Martian planetary heat flow have been performed, and estimates for the thermal state of the Martian interior rely on indirect methods (see, e.g., Grott and Breuer 2010 and references therein). Martian heat flow has been estimated from the deformation of the lithosphere under mechanical loads (e.g., Schultz and Watters, 2001, McGovern et al., 2004, Grott et al., 2005, Ruiz et al., 2009), yet large uncertainties are associated with this method. Interpretation of the heat flow estimates obtained is further complicated by the fact that the time of load emplacement does not necessarily represent the time the lithospheric shape was frozen-in, as lithospheric deformation will usually continue after loading is finished (Albert and Phillips, 2000, Brown et al., 2000). Further, the crater retention age of the corresponding surfaces may not represent the time of deformation (Beuthe et al., 2012), as they may have been overprinted by later activity. Therefore, direct heat flow measurements are needed to constrain the thermal state of Mars.

As Mars likely lacks present day plate tectonics (Breuer and Spohn, 2003) it can be considered geophysically less complex than the Earth, and it stands to reason that its average surface heat flow can – in analogy to the Moon – likely be constrained from measurements at only a few well-chosen sites. Surface heat flow variations are expected to be driven by differences of crustal thickness as well as the distribution of heat producing elements (Grott and Breuer, 2010), and these contributions can be estimated from models of crustal thickness (Zuber et al., 2000, Neumann et al., 2004) as well as gamma ray spectroscopy data (Taylor et al., 2006). Therefore, even a single measurement will serve as an important anchoring point for models of the Martian thermal evolution, and global estimates can be obtained by extrapolating the local measurement using numerical models (Plesa et al., 2015, 2016)

One example for a model of the present-day surface heat flow of Mars is shown in Figure 7, where heat flow is given as a function of geographical location. Present day heat flow has been estimated by calculating the thermal evolution of Mars starting after core formation to the present day using a 3-D mantle convection model. Estimates of crustal thickness (Neumann et al., 2004), the distribution of heat producing elements (Taylor et al., 2006), as well as their bulk abundance (Wänke and Dreibus, 1994) serve as model input. Calculated surface heat flow varies between 17 and 37 mW m^{-2} between the Hellas basin and the Tharsis province, respectively, and variations generally follow the trend imposed by the assumed crustal thickness, while mantle upwellings play a minor role. Note that the predicted areas of highest heat flow near Tharsis and Elysium coincide with areas for which volcanic resurfacing has been fairly recent (Neukum et al., 2004, Hauber et al., 2011) as would be expected.

The first in-situ heat flow measurement on the Martian surface will be performed by the InSight mission (Interior Exploration using Seismic Investigations, Geodesy and Heat Transport), and the InSight landing site is indicated by a white star in Figure 7. InSight carries the Heat Flow and Physical Properties Package HP^3 (Spohn et al., 2014), and an overview of the robotic lander and the main payload elements is shown in Figure 1 and Figure 8. HP^3 aims at constraining the surface heat flow at the landing site to within 5 mW m^{-2}, thus providing the first in-situ data point.

Image: DLR

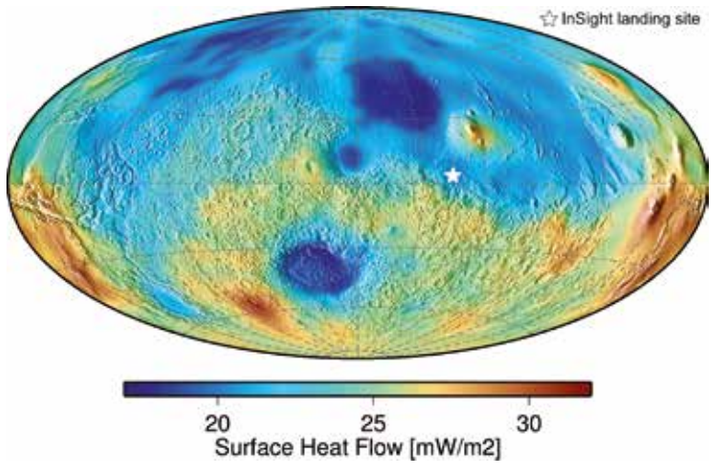

Figure 7: Theoretical Model of the Martian surface planetary heat flow as predicted by a thermal evolution model. A Wänke and Dreibus bulk composition of heat producing elements (Wänke and Dreibus, 1994) has been assumed. Models of the present-day crustal thickness (Neumann et al., 2004) as well as the distribution of heat producing elements between crust and mantle (Taylor et al., 2006) have been used as model inputs. The targeted landing site of the InSight mission is also indicated.

In contrast to the lunar measurements, heat flow measurements on Mars face some additional challenges: first and foremost, boreholes on Mars need to be deeper than they need to be on the Moon, as the regolith thermal

conductivity is larger, resulting in larger diurnal and annual skin depths. This is due to the presence of the Martian atmosphere, and gas in the regolith will considerably increase thermal conductivity as compared to atmosphere-less bodies (e.g., Huetter et al., 2008, Piqueux and Christensen 2009a, 2009b). Thus thermal conductivity is increased by a factor of two to five with respect to the lunar values.

Another difference between the upcoming Martian heat flow measurement and the Apollo experiments is the way the probe will be deployed: While the Apollo astronauts used hand-held rotary percussion drill systems to emplace the probes away from surface perturbations (Langseth, 1972, Heiken, 1991), the InSight probe will be placed onto the surface by a robotic arm with limited reach. Therefore, perturbations caused by the landing system and the lander itself need to be taken into account during data analysis (Grott, 2009, Kiefer, 2012). One of these perturbations is removal of surface dust during landing, as has been observed for the Phoenix and Curiosity landing sites (Daubar et al., 2015). Timescales for dust resettling have been estimated from HIRISE data as well as the re-brightening of rover tracks, and resettling can take up to a Martian year or longer. Aeolian sediment transport seems to be the dominant process for re-brightening (Geissler et al., 2010), while fallout of dust from the atmosphere seems to play only a minor role. These albedo changes as well as lander-induced shadows can have a significant influence on the surface radiative energy balance, and care must be taken to remove these contributions during data analysis.

Image: NASA/JPL-Caltech

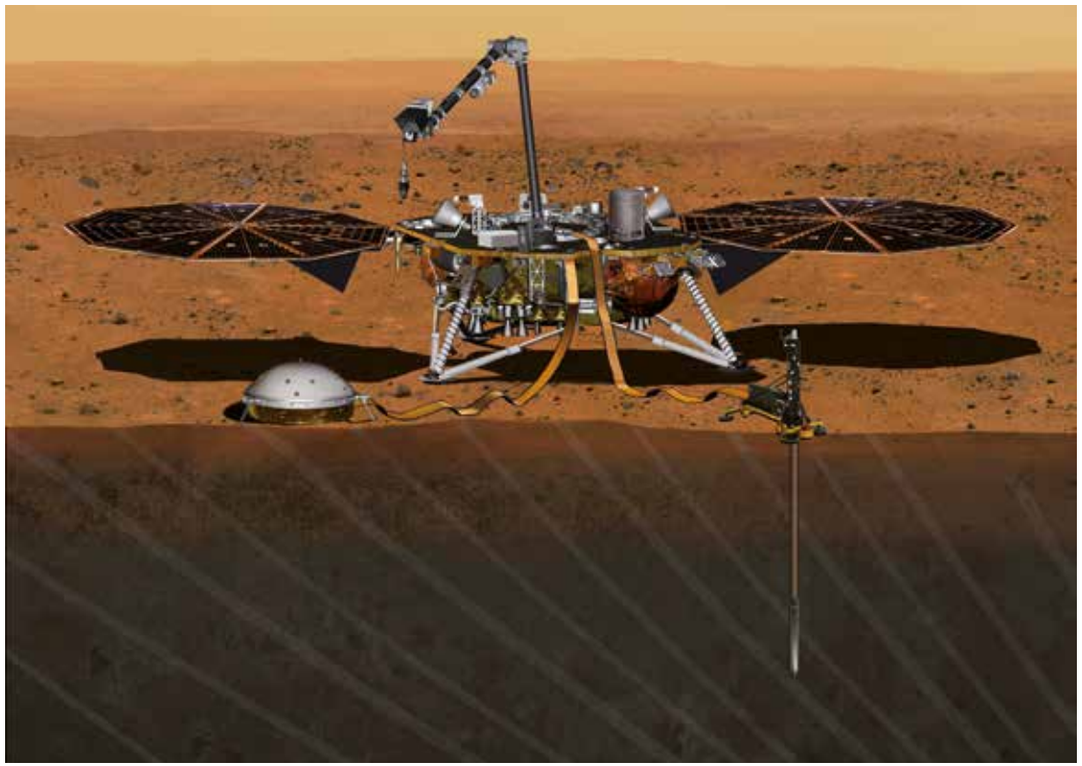

Figure 8: Sketch of the InSight Lander on the Martian surface. The lander's main instruments, i.e., the seismometer SEIS (left) as well as the Heat Flow and Physical Properties Package HP^3 (right) have been deployed onto the surface by the lander's robotic arm. The HP^3 mole has started penetration into the subsurface, deploying the science tether equipped with temperature sensors behind the mole. InSight will launch in May 2018 and reach Mars on November 26th, 2018.

Finally, the Martian spin axis lacks stabilization due to the absence of a large moon, and chaotic obliquity changes have been predicted from dynamical simulations (Laskar et al., 2004). These calculations are supported by geological evidence, which suggests that climate change on timescales of a few million years has occurred on Mars (Mustard et al., 2001, Kreslavsky et al, 2002, Head et al., 2003, Helbert et al., 2005). However, it has been shown that such long term signals have only a small effect on the subsurface thermal gradient (Grott et al., 2007), especially if an equatorial landing site is chosen (Mellon et al., 1992).

The Heat Flow and Physical Properties Package will address these challenges by emplacing temperature sensors to a targeted depth of 5 m using a mechanical hammering mechanism. In addition, the mechanism houses active heaters to determine regolith thermal conductivity in situ. Perturbations of the deployment site will be kept to a minimum by the robotic arm deployment, and the hammering action is expected to be less destructive than the Apollo rotary-percussion drill system. Surface perturbations caused by the landing and lander shadowing will be monitored by a dedicated surface temperatures sensor, the HP^3 radiometer, such that surface temperature perturbations can be quantified and taken into account during data analysis.

On Mars, HP^3 operations will consist of 10 hammering cycles. During each, the probe will advance 50 cm. After each cycle, heat accumulated during hammering will be allowed to dissipate for 2 days, before an active heating experiment to measure regolith thermal conductivity is conducted. In this way, a profile of thermal conductivity will be obtained, and temperature sensors will keep logging temperatures for a full Martian year. Depending on the thermal conductivity of the Martian regolith, annual surface temperature fluctuations may not have fully decayed at the target depth, but the extended measurement period of a full Martian year will allow for removing this signal from the data if present. Furthermore, any long-term drift can be monitored and the signal induced by lander shadowing can potentially be used to estimate regolith thermal diffusivity in addition to the direct in-situ thermal conductivity determination.

Summary and Conclusions

A planet's surface heat flow is a key quantity that describes the planet's thermal state and sheds light on the working of the planetary heat engine. While terrestrial heat flow measurements reflect the operation of plate tectonics, lunar heat flow indicates that the temperature inside of planetary bodies that operate in the stagnant lid regime of mantle convection is governed by the distribution of heat producing elements. This situation is also expected to be encountered on Mars, where the first extraterrestrial heat flow measurement since Apollo will be performed by InSight's Heat Flow and Physical Properties Package HP^3. HP^3 will constrain the heat flow at the landing site in Elysium Planitia to 5 mW m^{-2}, providing an important baseline measurement to constrain models of the Martian thermal evolution. The data to be obtained by HP^3 will thus be instrumental in understanding the history of Martian volcanism and have important implications for volcanic outgassing, the evolution of the Martian atmosphere, and thus the habitability of the planet during the Noachian and early Hesperian periods.

References

Albert, R.A., Phillips, R.J., Paleoflexure (2000), Geophysical Research Letters, Volume 27, Issue 16, p. 2385-2388, doi:10.1029/2000GL011816

Beardsmore, G. R., and J. P. Cull (2001), Crustal Heat Flow, Cambridge Univ. Press, Cambridge, U. K.

Beuthe, M., S. Le Maistre, P. Rosenblatt, M. Pätzold, V. Dehant, (2012), Density and lithospheric thickness of the Tharsis Province from MEX MaRS and MRO gravity data, Journal of Geophysical Research, Volume 117, Issue E4, E04002, doi:10.1029/2011JE003976

Breuer, D., Spohn, T., 2003. Early plate tectonics versus single-plate tectonics on Mars: Evidence from magnetic field history and crust evolution. J. Geophys. Res. 108 (E7), doi:10.1029/2002JE001999. 5072.

Brown, C.D., Phillips, R.J. (2000), Crust-mantle decoupling by flexure of continental lithosphere, Journal of Geophysical Research: Solid Earth, Volume 105, Issue B6, pp. 13,221-13,237, doi:10.1029/2000JB900069

Bullard, E. C. 1939. Heat flow in South Africa. Proc. Roy. Soc. London A 173, 474-502.

Bullard, E. 1954. The flow of heat through the floor of the Atlantic Ocean. Proc. Roy. Soc. London A 222, 408–429.

Christoffel, D. A. and Calhaem, I. M. 1969. A geothermal heat flow probe for in situ measurement of both temperature gradient and thermal conductivity.. J. Phys. E Scientific Instruments 2, 457–465.

Daubar, I.J., A. S. McEwen, and M. P. Golombek, Albedo Changes at Martian Landing Sites, 46th Lunar and Planetary Science Conference (2015), abstract 2225

Davies, J. H. (2013), Global map of solid Earth surface heat flow, Geochem. Geophys. Geosyst., 14, 4608–4622, doi:10.1002/ggge.20271.

Grasset, O., Parmentier, E.M., 1998. Thermal convection in a volumetrically heated, infinite Prandtl number fluid with strongly temperature-dependent viscosity: Implications for planetary evolution. J. Geophys. Res. 103, 18171–18181.

Grott, M., Helbert, J., Nadalini, R., 2007. Thermal structure of martian soil and the measurability of the planetary heat flow. J. Geophys. Res. 112, E09004. doi:10.1029/2007JE002905

Grott, M., 2009. Thermal disturbances caused by lander shadowing and the measurability of the martian planetary heat flow. Planet. Space Sci. 57, 71–77.

Grott, M., E. Hauber, S. C. Werner, P. Kronberg, and G. Neukum (2005), High heat flux on ancient Mars: Evidence from rift flank uplift at Coracis Fossae, Geophys. Res. Lett., 32, L21201, doi:10.1029/2005GL023894.

Grott, M., and D. Breuer (2010), On the spatial variability of the Martian elastic lithosphere thickness: Evidence for mantle plumes?, J. Geophys. Res., 115, E03005, doi:10.1029/2009JE003456.

Fraeman A. A. and Korenaga J. 2010. The influence of mantle melting on the evolution of Mars. Icarus 210:43–57.

Hauber, E., Brož, P., Jagert, F., Jodłowski, P., Platz, T. (2011), Very recent and wide-spread basaltic volcanism on Mars, Geophysical Research Letters, 38, 10, L10201, doi:10.1029/2011GL047310

Hagermann, A., Planetary heat flow measurements, Royal Society of London Transactions Series A, vol. 363, Issue 1837, p.2777-2791, 2005, doi:10.1098/rsta.2005.1664

Head, J. W., J. F. Mustard, M. A. Kreslavsky, R. E. Milliken, and D. R. Marchant (2003), Recent ice ages on Mars, Nature, 426(6968), 797– 802.

Helbert, J., D. Reiss, E. Hauber, and J. Benkhoff (2005), Limits on the burial depth of glacial ice deposits on the flanks of Hecates Tholus, Mars, Geophys. Res. Lett., 32, L17201, doi:10.1029/2005GL023712.

Heiken, G., D. Vaniman, and B. French (Eds.) (1991), Lunar Sourcebook, Cambridge Univ. Press, Cambridge, U. K.

Hütter, E. S., N. I. Koemle, G. Kargl, and E. Kaufmann (2008), Determination of the effective thermal conductivity of granular materials under varying pressure conditions, J. Geophys. Res., 113, E12004, doi:10.1029/2008JE003085.

Walter S.Kiefer nLunar heat flow experiments: Science objectives and a strategy for minimizing the effects of lander-induced perturbations, Planetary and Space Science 60 (2012) 155–165, 2012

Korenaga J. 2009. Scaling of stagnant-lid convection with Arrhenius rheology and the effects of mantle melting. Geophysical Journal International 179:154–170.

Kreslavsky, M. A., and J. W. Head III (2002), Mars: Nature and evolution of young latitude-dependent water-ice-rich mantle, Geophys. Res. Lett., 29(15), 1719, doi:10.1029/2002GL015392.

Laneuville, M., M. A. Wieczorek, D. Breuer, and N. Tosi (2013), Asymmetric thermal evolution of the Moon, J. Geophys. Res. Planets, 118, 1435–1452, doi:10.1002/jgre.20103.

Langseth, M. G., S. P. Clark, J. L. Chute, S. J. Keihm, and A. E. Wechsler (1972a), Heat flow experiment, in Apollo 15: Preliminary Science Report, Rep. SP-289, pp. 1–23, chap. 11, Natl. Aeronaut. and Space Admin., Washington, D. C.

Langseth, M. G., S. P. Clark, J. L. Chute, S. J. Keihm, and A. E. Wechsler (1972b), The Apollo 15 lunar heat-flow measurement, Earth Moon Planets, 4(3–4), 390–410, doi:10.1007/BF00562006.

Langseth, M. G., S. J. Keihm, and J. L. Chute (1973), Heat flow experiment, in Apollo 17: Preliminary Science Report, Rep. SP-330, pp. 1–24, chap. 9, Natl. Aeronaut. and Space Admin., Washington, D. C.

Langseth, M. G., S. J. Keihm, and K. Peters (1976), Revised lunar heatflow values, Proc. Lunar Sci. Conf., 7th, 7, 3143–3171.

Laskar, J., A. C. M. Correia, M. Gastineau, F. Joutel, B. Levrard, and P. Robutel (2004), Long term evolution and chaotic diffusion of the insolation quantities on Mars, Icarus, 170, 343– 364.

Lister, C. R. B. 1970. Measurement of the in situ sediment conductivity by means of a Bullard–type probe. Geophys. J. R. astr. Soc. 19, 521–532.

Lodders, K., and B. Fegley (1997), An oxygen isotope model for the composition of Mars, Icarus, 126(2), 373–394.

McGovern, P. J., S. C. Solomon, D. E. Smith, M. T. Zuber, M. Simons, M. A. Wieczorek, R. J. Phillips, G. A. Neumann, O. Aharonson, and J. W. Head (2004), Correction to "Localized gravity/topography admittance and correlation spectra on Mars: Implications for regional and global evolution," J. Geophys. Res., 109, E07007, doi:10.1029/2004JE002286.

Mellon, M. T., and B. M. Jakosky (1992), The effects of orbital and climatic variations on Martian surface heat flow, Geophys. Res. Lett., 19(24), 2393–2396.

Morgan, J. W., and E. Anders (1979), Chemical composition of Mars, Geochim. Cosmochim. Acta, 43(10), 1601–1610, doi:10.1016/0016-7037(79)90180-7.

Mustard, J. F., C. D. Cooper, and M. K. Rifkin (2001), Evidence for recent climate change on Mars from the identification of youthful near-surface ground ice, Nature, 412, 411 – 414.

Neukum, G., Jaumann, R., Hoffmann, H., Hauber, E., Head, J.W., Basilevsky, A.T., Ivanov, A.B., Werner, S.C., van Gasselt, S., Murray, J.B., McCord, T., the HRSC Co-Investigator Team, 2004. Recent and episodic volcanic and glacial activity on Mars revealed by the High Resolution Stereo Camera. Nature 432, 971–979. 7020.

Spohn, T., M. Grott, S. Smrekar, C. Krause, T.L. Hudson, and the HP3 instrument team (2014) Measuring the Martian Heat Flow using the Heat Flow and Physical Properties Package (HP3), 46th Lunar and Planetary Science Conference, abstract 1916.

Neumann, G.A., Zuber, M.T., Wieczorek, M.A., McGovern, P.J., Lemoine, F.G., Smith, D.E., 2004. Crustal structure of Mars from gravity and topography. J. Geophys. Res. 109, doi:10.1029/2004JE002262. E08002.

Piqueux, S., and P. Christensen (2009a), A model of thermal conductivity for planetary soils: 1. Theory for unconsolidated soils, J. Geophys. Res., 114, E09005, doi:10.1029/2008JE003308.

Piqueux, S., and P. Christensen (2009b), A model of thermal conductivity for planetary soils: 2. Theory for cemented soils, J. Geophys. Res., 114, E09006, doi:10.1029/2008JE003309.

Plesa A.-C., Tosi N., Grott M., and Breuer D. 2015. Thermal evolution and Urey ratio of Mars. Journal of Geophysical Research—Planets 120:995–1010.

Plesa, A.-C.; M. Grott, N. Tosi, D. Breuer, T. Spohn, and M. Wieczoreck (2016): How large are present-day heat flux variations across the surface of Mars? In: JGR Planets, Vol. 121(12), pp. 2386-2403, doi:10.1002/2016JE005126.

Pollack, H., S. Hurter, and J. Johnson (1993), Heat flow from the Earth's interior: Analysis of the global dataset, Rev. Geophys., 31(3), 267–280.

Rasmussen, K. L., and P. H. Warren (1985), Megaregolith thickness, heat flow, and the bulk composition of the Moon, Nature, 313, 121–124, doi:10.1038/313121a0.

Reese, C.C., Solomatov, V.S., Moresi, L.-N., 1998. Heat transport efficiency for stagnant lid convection with dislocation viscosity: Application to Mars and Venus. J. Geophys. Res. 103 (E6), 13643–13658. doi:10.1029/98JE01047.

Ruiz, J., J.-P. Williams, J. M. Dohm, C. Fernández, and V. López (2009), Ancient heat flow and crustal thickness at Warrego rise, Thaumasia highlands, Mars: Implications for a stratified crust, Icarus, 203, 47–57,

doi:10.1016/j.icarus.2009.05.008.

Saito, Y., S. Tanaka, J. Takita, K. Horai, and A. Hagermann (2007), Lost Apollo heat flow data suggest a different bulk lunar composition, Lunar Planet. Sci., XXXVII, Abstract 2197.

Saito, Y., S. Tanaka, K. Horai, and A. Hagermann (2008), The long term temperature variation in the lunar subsurface, Lunar Planet. Sci., XXXIX, Abstract 1663.

Schubert, G., Cassen, P., Young, R.E., 1979. Subsolidus convective cooling histories of terrestrial planets. Icarus 38, 192–211. doi:10.1016/0019-1035(79)90178-7.

Schubert, G. and Spohn, T. (1990). Thermal history of Mars and the sulfur content of its core. J. Geophys. Res., 95, 14,095–14,104.

Schultz, R.A.,Watters, T.R., 2001. Forward mechanical modeling of the Amenthes Rupes thrust fault on Mars. Geophys. Res. Lett. 28, 4659–4662.

Solomatov, V.S., Moresi, L.N., 1997. Three regimes of mantle convection with non-Newtonian viscosity and stagnant lid convection on the terrestrial planets. Geophys. Res. Lett. 24 (15), 1907–1910. doi:10.1029/97GL01682.

Spohn, T., 1991. Mantle dilerentiation and thermal evolution of Mars, Mercury, and Venus. Icarus 90, 222–236.

Spohn, T, and G. Schubert, Convective thinning of the lithosphere - A mechanism for the initiation of continental rifting, Journal of Geophysical Research, vol. 87, 1982, p. 4669-4681, doi:10.1029/JB087iB06p04669

Stevenson, D.J., Spohn, T., Schubert, G., 1983. Magnetism and thermal evolution of the terrestrial planets. Icarus 54, 466–489.

Taylor, G.J., Boynton, W., Brückner, J., Wänke, H., Dreibus, G., Kerry, K., Keller, J., Reedy, R., Evans, L., Starr, R., Squyres, S., Karunatillake, S., Gasnault, O., Maurice, S., d'Uston, C., Englert, P., Dohm, J., Baker, V., Hamara, D., Janes, D., Sprague, A., Kim, K., Drake, D., 2006. Bulk composition and early differentiation of Mars. J. Geophys. Res. 111 (E3), doi:10.1029/2005JE002645. E03S10.

Treiman, A. H., M. J. Drake, M.-J. Janssens, R. Wolf, and M. Ebihara (1986), Core formation in the Earth and Shergottite Parent Body (SPB): Chemical evidence from basalts, Geochim. Cosmochim. Acta, 50(6), 1071–1091, doi:10.1016/0016-7037(86)90389-3.

Wänke, H., and G. Dreibus (1994), Chemistry and accretion of Mars, Philos. Trans. R. Soc. London, A349, 2134–2137.

Warren, P. H., and K. L. Rasmussen (1987), Megaregolith insulation, internal temperatures, and bulk uranium content of the Moon, J. Geophys. Res., 92, 3453–3465, doi:10.1029/JB092iB05p03453.

Wieczorek, M. A., and R. J. Phillips (2000), The "Procellarum KREEP Terrane": Implications for mare volcanism and lunar evolution, J. Geophys. Res., 105, 20,417–20,430, doi:10.1029/1999JE001092.

Wieczorek, M., and S. Huang (2006), A reanalysis of Apollo 15 and 17 surface and subsurface temperature series, Lunar Planet. Sci., XXXVII, Abstract 1682.

Zuber, M.T., Solomon, S.C., Phillips, R.J., Smith, D.E., Tyler, G.L., Aharonson, O., Balmino, G., Banerdt, W.B., Head, J.W., Johnson, C.L., Lemoine, F.G., McGovern, P.J., Neumann, G.A., Rowlands, D.D., Zhong, S., 2000. Internal structure and early thermal evolution of Mars from Mars global surveyor topography and gravity. Science 287, 1788–1793.